A MICROTIP EQUIPPED BIDIRECTIONAL MICROROBOT FOR NAVIGATING ON AND PENETRATING A LEAF SURFACE

Tony H. Wang, Dea Gyu Kim, Zhijian Hao, and Azadeh Ansari
School of Electrical and Computer Engineering, Georgia Institute of Technology, Atlanta, Georgia, USA

ABSTRACT

This work presents a novel, magnetically actuated, micro-scale robot (with dimensions of 100μm × 112μm × 44μm), equipped with a 43μm long microtip. Under an out-of-plane, sawtooth magnetic wave, the robot undergoes stick-slip motion about its rockers with speeds up to 140μm/s and can travel either forward or backward via introducing a magnetic field offset. When subject to a static, out-of-plane magnetic field, the microrobot upends on its tip and can penetrate leaf tissue, demonstrating selective tip engagement and potential biomedical applications such as drug delivery and DNA extraction.

KEYWORDS

Microrobots, magnetic actuation, microtip, stick-slip motion

INTRODUCTION

Microscale robots (microrobots) show promise for biomedical applications such as drug delivery [1, 2] and microsurgery [3] due to their smaller sizes, less invasive nature, and higher capabilities of maneuvering precisely in narrow and otherwise inaccessible spaces when compared to conventional robots. As the powering provided by on-board batteries becomes insufficient at microscale [4], current methods of microrobot actuation mainly consist of off-board approaches such as magnetic fields, acoustic excitation, electric fields, and optical/thermal heating.

From a biomedical application perspective, magnetic fields are the most attractive approach due to their penetration through tissue, good biocompatibility, and higher steering capabilities. In [1], Lee et al. designed and fabricated a nickel-coated, helical microrobot with a needle to attach onto microtissues for drug delivery. When coated with a biocompatible material such as titanium [2], microrobots could grow stem-cells on their structures and act as transporters. Microrobots with higher remanent magnetic materials, such as neodymium, can penetrate as well as drill through tissue [3] for microsurgical purposes.

Current magnetic setups often utilize multi-axis electromagnetic coils to generate magnetic fields, such as rotational magnetic fields, for motion manipulation. Examples include Helmholtz coils, which enforce uniform magnetic fields, and Maxwell coils, which generate uniform magnetic gradients. While these systems are used extensively in magnetic microrobot literature, their use of multiple in-plane (IP) and out-of-plane (OOP) coils limit the working space of the microrobots to the confines of the electromagnets. This proves disadvantageous if such a setup needs to be placed under a microscope of limited focal length or incorporated around a patient. A more simplistic system, demonstrating the same capabilities as the previous examples, is necessary to advance the range of applications for microrobots.

In this work, we present a microrobot (100μm × 112μm × 44μm) equipped with a 43μm long microtip and capable of bidirectional motion from a single electromagnet. 3D printed via two-photon polymerization (2PP), the microrobot (Figure 1a) consists of a main polymeric body deposited with a nickel thin film and two rocker-like contacts and will henceforth be named the microrocker bot. Under an OOP, static magnetic field within ±1mT provided by the electromagnet, the microrocker bot tilts either forward (with positive offset) or backward (with negative offset) to align its magnetization, biasing its position towards either direction. Outside this range, the microrocker bot completely upends on its front or back for potential tip engagement, demonstrating a new actuation mode (Figure 1b). When the static field is used as a small offset combined with an oscillating magnetic waveform, the robot can travel either forward or backward (Figure 1c) with speeds up to 140μm/s on glass

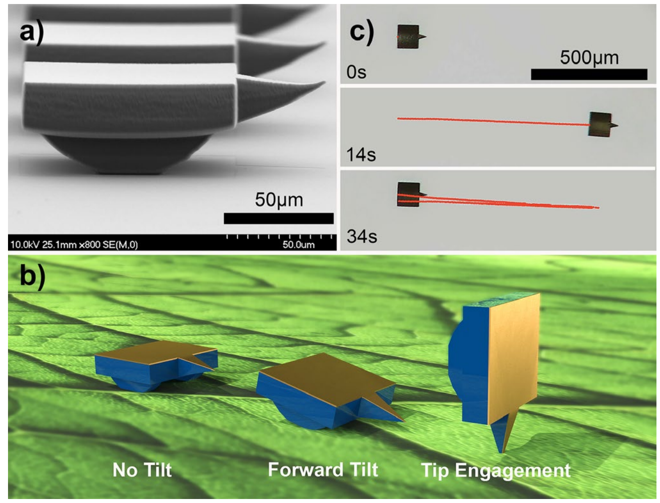

Figure 1: a) Side SEM view of the microrobot. b) A schematic depicting the positional biases of the microrobot from a magnetic offset. The nickel thin film is colored gold while the main body is colored blue. c) Tracked forward and backward motion of the microrobot on glass under a 16Hz oscillating OOP magnetic field.

Additionally, the microrobot could demonstrate bidirectional motion on the biological, rougher surface of a leaf (*Lysimachia nummularia*). When induced with sufficient magnetic field amplitude, the microrocker bot penetrated the leaf surface via upending on its microtip. Such a result provides insights into possible applications for drug delivery and plant DNA extraction.

BACKGROUND

Magnetic actuation

For soft magnetic materials such as nickel, the easy axis of magnetization, defined as the preferred direction for spontaneous magnetization in ferromagnets, lies along their longest dimension if they are geometrically anisotropic [4]. As a result, the nickel thin film's primary magnetization direction will not run along its thickness. Relative to the robot's body, the preferred magnetic orientation of the thin film is front-to-back instead of side-to-side, allowing the robot to pivot about its rockers for forward and backward motion. This can be explained by the different internal stresses present in the front-to-back and side-to-side directions. Due to 3D printing, the top surface of the robot's body consists of raster lines running parallel to the side-to-side direction, which create a higher stress distribution than the front-to-back direction. This will affect the magnetic strain energy density E_s, which is expressed as [5]:

$$E_s = \frac{3}{2}\lambda\sigma \sin^2\theta_t, \qquad (1)$$

where λ is the saturation magnetostriction constant, σ is the film stress, and θ_t is the angle that the raster lines make with the IP direction. Due to the positive tensile stress present in the thin film for both IP directions as well as the negative magnetostriction constant present in nickel, the overall energy density is negative and signifies that the magnetization is decreased by tension. Consequently, the easy axis of magnetization lies in the front-to-back orientation of the robot due to its lower tensile stress.

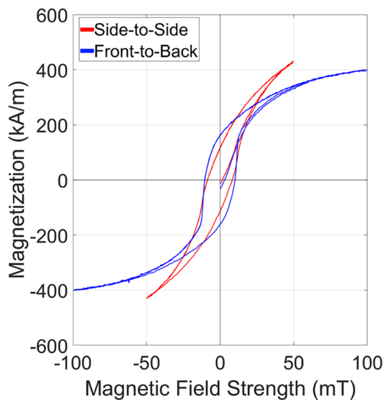

Figure 2: Magnetic hysteresis loop

For characterization, the magnetic properties of the nickel thin film were measured by placing a microrobot inside a vibrating-sample magnetometer. Figure 2 shows the hysteresis loops for two magnetization directions: the robot's front-to-back and side-to-side orientations. The higher coercivity (10.5 > 8.6mT) and retentivity (160 > 115kA/m) values of the front-to-back loop confirms that the easy axis of the nickel thin film lies in that direction. The saturation magnetization of the front-to-back orientation is 400kA/m, which will be used to calculate the maximum force and torque the microtip can exert for penetrating the leaf surface.

Under a magnetic field $\boldsymbol{B}$, the microrocker bot will experience a torque $\boldsymbol{T}$ and force $\boldsymbol{F}$ expressed as:

$$\boldsymbol{T} = V_m \boldsymbol{M} \times \boldsymbol{B} \quad (2)$$

$$\boldsymbol{F} = V_m \boldsymbol{M} \cdot \nabla \boldsymbol{B} \quad (3)$$

where V_m and $\boldsymbol{M}$ are the magnetic material's volume and magnetization vector respectively.

Stick-slip motion

To induce stick-slip motion, a sawtooth waveform is provided from a function generator to the electromagnet for an OOP pulsing magnetic field. The slow ramp and steep decay in a sawtooth wave period correspond to the stick and slip phases respectively, as the instantaneous change in field direction maximizes the robot's rotation during slip phase. For bidirectional motion, a small DC offset can be introduced in the waveform to positionally bias the robot either forward or backward.

Stick-slip motion involves multiple forces and torques that the robot experiences, which primarily include magnetic force and torque, adhesion, drag forces, and kinetic and static friction forces. The OOP magnetic torque during the steep decay of the sawtooth wave causes an increase in angular acceleration as the robot attempts to align its magnetization to the external field. When this acceleration becomes sufficiently high, the rocker's point of contact overcomes the static friction force. Since the robot's angular motion is coupled with its rocker motion, this acceleration allows the robot to enter its slip phase for net motion. For quantitative modeling and simulation of the microrocker bot's stick-slip motion, readers are referred to our previous work [6].

EXPERIMENTAL DESIGN

Fabrication

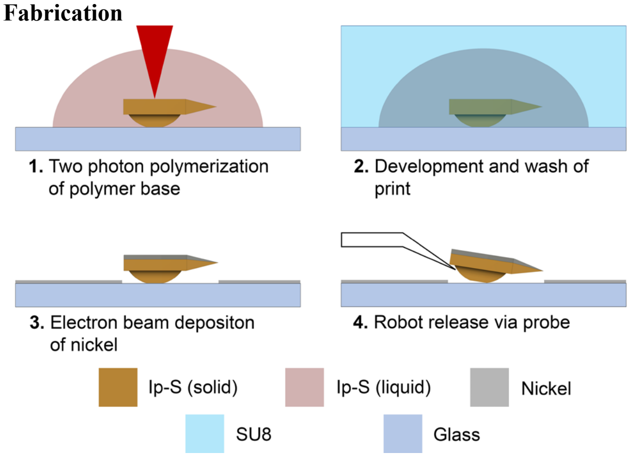

Figure 3: Fabrication process

The microrocker bots were 3D printed via two-photon polymerization on a Nanoscribe Photonic Professional GT printer. Figure 3 details the process. First, a drop of Ip-S photoresin was deposited on an indium tin oxide layered glass slide and loaded into the printer. A 25x objective lens was used for direct laser writing, which serially polymerized the photoresin at the laser's focal point. After the print was finished, the microrobots were developed in SU8 solution for 20 minutes and washed in isopropanol alcohol (IPA) for 2 minutes. For magnetic actuation, the robots were deposited with a 300nm nickel layer through electron beam deposition. Finally, a probe was used to release the microrobots from the surface.

Experimental setup

After release, the robots were transferred to the substrate through a micropipette. While the microrobots could move on the substrate in air, the sample was submerged in water to record more consistent motion and lower adhesion. The sample was then placed on top of 8cm diameter and 9.5mm thick cylindrical electromagnet (Kaka Electronics KK-P25), which was connected to a function generator (Agilent 33220-A). The robots were imaged by a Moticam 1080 camera connected to a top-down microscope (MPI TS150-THZ) and tracked via the DLTdv digitizing tool for video processing [7]. For all experiments, a 10V_{pp} sawtooth magnetic waveform with a ±150mV offset was supplied to the electromagnet, which corresponded to an OOP magnetic field amplitude of 3.10mT_{pp}. and an offset of ±50µT.

RESULTS AND DISCUSSION

Robot speed on glass

To characterize speed, the robot's forward and backward trajectories on a glass slide were recorded from 4Hz to 50Hz in 2Hz increments. As shown in Figure 4, there is a clear speed-frequency variation for forward and backward motions. At lower frequencies, the microrobots oscillate less over a set time, leading to less slip phases and reduced speeds. Meanwhile, at higher frequencies, the faster duty cycles cause higher torsional and translational damping, leading to slower speeds.

Due to the geometric differences between the front and back of the robot, the two plots show significantly different responses to the applied frequencies. The microrocker bot achieves a peak forward speed of 80µm/s at 12Hz and a peak backward speed of 140µm/s at 20Hz. The robot's front microtip limits forward rocking and consequently the amount of angular acceleration the robot can undergo for forward motion, reducing robot speed.

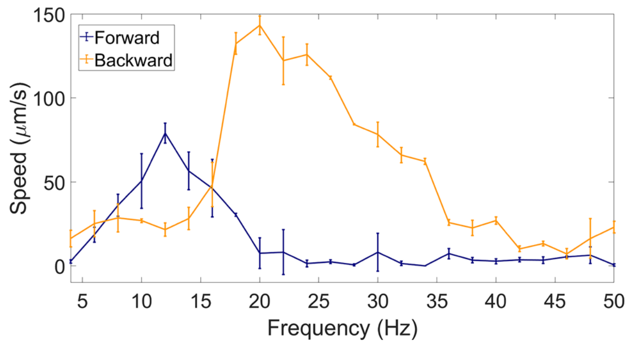

Figure 4: Speed-frequency plot for forward/backward motions. The error bars represent the standard deviation from 3 trials.

The inclusion of a tip additionally explains the different speed-frequency distributions for the two directions. Lower frequencies have longer period cycles and thereby allow the robot to undergo larger displacements. For forward motion, this lower frequency range (8-18Hz) provides a longer response time for the robot to align its magnetization during stick phase, achieving larger displacements and gaining enough angular acceleration during slip phase to overcome the front tip's obstruction to motion. Alternatively, while higher frequencies (20-50Hz) provide faster duty cycles, the lower displacement amplitudes as well as the positional bias from the static magnetic offset cause the tip to become pinned onto the substrate and significantly slow down the robot's speed in comparison to backward motion. This behavior at higher frequencies can be tuned by decreasing the static offset used for forward motion; however, such a change will also bias the neutral position less and change the speed-frequency response. As a result, offset optimization is needed in the future to obtain the best balance between speed and viable frequency range.

Robot motion on a leaf and tip engagement

For mobility on biological surfaces, the microrocker bot was placed on a 2cm diameter leaf and actuated at 12Hz for forward motion and 20Hz for backward motion, corresponding to the peak responses observed in Figure 5. While the robots were able to travel forward and backward, their speeds were reduced with forward and backward speeds reaching 49±6.3µm/s and 54±5.7µm/s respectively from 3 trials. This reduction in speed can be attributed to the uneven and rougher surface of the leaf, which is due to the veins, trichomes, and waxes present [8], and highlights the sensitivity of stick-slip motion to surface inhomogeneities. Faster speeds will require increasing the magnetic field amplitude to induce larger amplitudes for greater angular acceleration.

Additionally, the robot can engage its tip on the leaf surface under a 5mT static field, as the robot has unlimited response time to completely align its magnetization (Figure 5). This result expands upon the static offset control shown in [6] and demonstrates a separate mode from stick-slip motion using a single electromagnet. When upending, the microrobot first rotates about its rockers and then transfers its point of contact to the microtip. As a result, the range of tip engagement can be approximated as 100µm, the distance between the rocker flat edge and microtip, and shows potential applications for precise drug delivery injection.

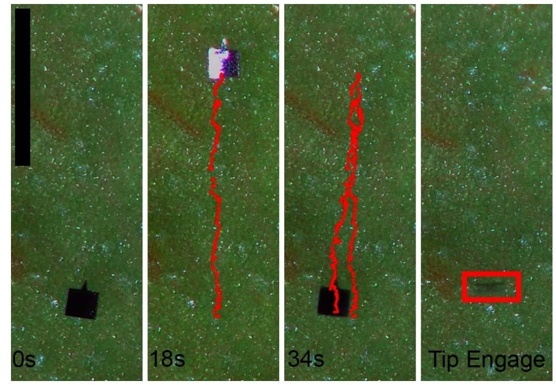

Figure 5: Tracked trajectory of the microrocker bot on a leaf. The tip engagement mode is emphasized due to limited visibility. The black scale bar has a length of 500µm.

Microtip penetration into leaf

To test microtip penetration, a stack of four 2.8cm diameter neodymium magnets was brought underneath the leaf surface for the microrocker bots to engage their tips. The magnetic field strength at the surface of the magnet's center was measured by a Hall effect sensor as 230mT, a value beyond the saturation field strength values (Figure 2) indicated in the hysteresis curve. To calculate the field gradient, the magnetic field amplitudes were measured at varying distances from the magnet's center, and the maximum field gradient was found to be 12T/m. After 5 minutes, the magnet was removed, and the sample was sputtered with 5nm of gold and observed under an SEM.

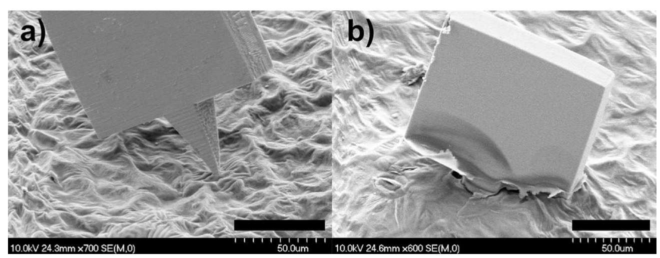

Figure 6: a) 5µm vs. b) full microtip penetration into the leaf. The black scale bar is 500µm in length.

Notably, the SEM photos of the two microrocker bots show very different levels of penetration, with robot 1 (Figure 6a) showing ~4µm of penetration and robot 2 (Figure 6b) showing near complete penetration into the leaf surface. This difference in penetration can be attributed to the different locations of the two robots relative to the magnet's center. While robot 1 was found at the center of the leaf, robot 2 was found at the leaf's edge and consequently experienced magnetic fringing at the magnet's edges. The field strength and gradient at the edge was measured and calculated as 340mT and 24T/m, which caused 150% and 200% increases in torque and force relative to the magnet's center respectively. Since peak force occurs at the critical transition between indentation and penetration of soft solids, additional depth afterwards is more easily achieved due to the lower work of penetration relative to the work of indentation [9]. Despite their variability, these results nonetheless demonstrate that microtip penetration into biological tissue is possible via simply placing a highly magnetic material near the microrocker bots.

Simulation of microtip mechanics

The microtip's mechanical interaction with the leaf surface was simulated via finite element analysis (FEA) on COMSOL Multiphysics 5.5. Here, the contact between the microtip and leaf substrate was assumed to be quasistatic and frictionless. Based on previous literature characterizing the mechanical properties of leaves [10, 11], the elastic modulus E and Poisson's ratio ν of the leaf were approximated as 2MPa and 0.4 respectively. The microtip itself was modeled as a conical structure with the material properties of Ip-S photoresin ($E = 4.6$GPa, $\nu = 0.3$) and a flat end diameter of 1.35μm based on SEM images.

For magnetic microrobots, magnetic forces typically have a smaller effect in terms of robot actuation than magnetic torques [4]. Applying the magnetic field and gradient values from the magnet's center as well as the nickel thin film's saturation magnetization to Eq. 3, the magnetic force $\boldsymbol{F_g}$ due to gradient can be calculated as 17nN. To calculate the force $\boldsymbol{F_t}$ applied due to torque $\boldsymbol{T}$, the lever at which $\boldsymbol{T}$ acts upon is the distance vector $\boldsymbol{d}$ between the microtip's edge and the front rocker edge since the robot will initially pivot about its front rocker. At a rotation angle of 20°, the microtip will contact the substrate at a torque of 300μN·μm from Eq. 2. By dividing this torque magnitude by the lever arm length $|\boldsymbol{d}| = \mathbf{100}$μm, $\boldsymbol{F_t}$ can be calculated as 3μN, which is two orders of magnitude higher than $\boldsymbol{F_g}$.

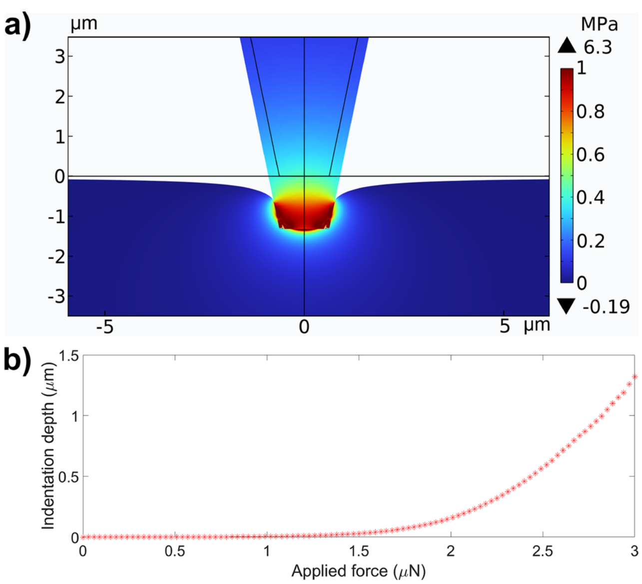

Figure 7: a) Indentation and pressure profile of microtip indentation into leaf. b) Simulated indentation depth vs. force.

Figure 7a shows the maximum pressure exerted by the microtip on the leaf surface. At 6.3MPa, the microtip deforms the leaf surface by 1.3μm. At smaller magnetic forces and torques, the microtip exerts less pressure and cannot deform the mesh, showing a threshold for the applied force. Figure 7b captures this nonlinear relationship between the force and indentation depth. Beyond 1.5μN, the indentation depth notably rises more with increasing forces. At a critical depth [9], the microtip transitions from indentation to penetration when the work of indentation equals to the work of penetration. During penetration, the onset of crack propagation allows microtip to slip into the crack and lowers the required force for penetration as the surrounding tissue relaxes.

CONCLUSION

This work presents a microrobot capable of stick-slip motion via a single electromagnet and mechanical penetration of a biological substrate. This novel method of actuation utilizes a static DC offset in the OOP magnetic field, which biases the robot's position to either travel forward or backward. Additionally, the same motion could be performed on the rougher, more inhomogeneous surface of a leaf, showing proof of concept for traveling on biological substrates to perform drug delivery or DNA extraction by using its microtip for penetration.

Future work will investigate the tip engagement mode of the microrobot as well as coating the microtip with biocompatible materials for potential stem cell delivery. Additionally, motion capabilities will be studied more in dry air environments for more flexibility. Overall, these initial results demonstrate precise steering and tip penetration of an untethered microrobot, opening a wide range of potential biomedical applications.

ACKNOWLEDGEMENTS

This work is supported by the National Science Foundation Graduate Research Fellowship under Grant No. DGE-1650044. The authors thank Prof. Martin Mourigal for magnetic characterization.

REFERENCES

[1] S. Lee, J. Kim, J. Kim, A. K. Hoshiar, J. Park, S. Lee, J. Kim, S. Pané, B. J. Nelson, and H. Choi, "A needle-type microrobot for targeted drug delivery by affixing to a microtissue," Advanced Healthcare Materials, vol. 9, no. 7, 2020.

[2] S. Jeon, S. Kim, S. Ha, S. Lee, E. Kim, S. Y. Kim, S. H. Park, J. H. Jeon, S. W. Kim, C. Moon, B. J. Nelson, J.-young Kim, S.-W. Yu, and H. Choi, "Magnetically actuated microrobots as a platform for Stem Cell Transplantation," Science Robotics, vol. 4, no. 30, 2019.

[3] D. Li, M. Jeong, E. Oren, T. Yu, and T. Qiu, "A helical microrobot with an optimized propeller-shape for propulsion in viscoelastic biological media," Robotics, vol. 8, no. 4, 2019.

[4] E. Diller and M. Sitti, Micro-scale mobile robotics. Foundation and Trends in Robotics, vol. 2, no. 3, 2013.

[5] M. Satō, K. Mukasa, and M. Maeda, "Uniaxial magnetic anisotropy in nickel-iron thin films electrodeposited on scratched surfaces," Japanese Journal of Applied Physics, vol. 8, no. 4, pp. 468–472, 1969.

[6] T.H. Wang, D. Kim, Y. Shi, Z. Hao, and A. Ansari, "Bidirectional microscale rocker robots controlled via neutral position offset", Journal of Micro-Bio Robotics, 2022.

[7] T. L. Hedrick, "Software techniques for two- and three-dimensional kinematic measurements of biological and Biomimetic Systems," Bioinspiration & Biomimetics, vol. 3, no. 3, 2008.

[8] H. Bediaf, R. Sabre, L. Journaux, and F. Cointault, "Comparison of leaf surface roughness analysis methods by sensitivity to noise analysis," Biosystems Engineering, vol. 136, pp. 77–86, 2015.

[9] S. Fregonese and M. Bacca, "Piercing soft solids: A mechanical theory for needle insertion," Journal of the Mechanics and Physics of Solids, vol. 154, 2021.

[10] Y. Onoda, F. Schieving, and N. P. Anten, "A novel method of measuring leaf epidermis and mesophyll stiffness shows the ubiquitous nature of the sandwich structure of leaf laminas in broad-leaved angiosperm species," Journal of Experimental Botany, vol. 66, no. 9, 2015.

[11] W. Zhang, P. Soman, K. Meggs, X. Qu, and S. Chen, "Tuning the Poisson's ratio of biomaterials for investigating cellular response," Advanced Functional Materials, vol. 23, no. 25, 2013.